Developmental changes in the cochlear hair cell mechanotransducer channel and their regulation by transmembrane channel–like proteins

Kyunghee X. Kim and Robert Fettiplace

Department of Neuroscience, University of Wisconsin-Madison, WI 53706

Vibration of the stereociliary bundles activates calcium-permeable mechanotransducer (MT) channels to initiate sound detection in cochlear hair cells. Different regions of the cochlea respond preferentially to different acoustic frequencies, with variation in the unitary conductance of the MT channels contributing to this tonotopic organization. Although the molecular identity of the MT channel remains uncertain, two members of the transmembrane channel–like family, Tmc1 and Tmc2, are crucial to hair cell mechanotransduction. We measured MT channel current amplitude and Ca^{2+} permeability along the cochlea's longitudinal (tonotopic) axis during postnatal development of wild-type mice and mice lacking Tmc1 (*Tmc1−/−*) or Tmc2 (*Tmc2−/−*). In wild-type mice older than postnatal day (P) 4, MT current amplitude increased ∼1.5-fold from cochlear apex to base in outer hair cells (OHCs) but showed little change in inner hair cells (IHCs), a pattern apparent in mutant mice during the first postnatal week. After P7, the OHC MT current in *Tmc1−/−* (*dn*) mice declined to zero, consistent with their deafness phenotype. In wild-type mice before P6, the relative Ca^{2+} permeability, P_{Ca}, of the OHC MT channel decreased from cochlear apex to base. This gradient in P_{Ca} was not apparent in IHCs and disappeared after P7 in OHCs. In *Tmc1−/−* mice, P_{Ca} in basal OHCs was larger than that in wild-type mice (to equal that of apical OHCs), whereas in *Tmc2−/−*, P_{Ca} in apical and basal OHCs and IHCs was decreased compared with that in wild-type mice. We postulate that differences in Ca^{2+} permeability reflect different subunit compositions of the MT channel determined by expression of Tmc1 and Tmc2, with the latter conferring higher P_{Ca} in IHCs and immature apical OHCs. Changes in P_{Ca} with maturation are consistent with a developmental decrease in abundance of Tmc2 in OHCs but not in IHCs.

The Journal of General Physiology

INTRODUCTION

Hair cells, the sensory receptors of the cochlea, detect sounds through deflection of their stereociliary bundles, which activates mechanotransducer (MT) ion channels. MT channels, calcium-permeable cation channels (Corey and Hudspeth, 1979; Ohmori, 1985; Beurg et al., 2006) with large (>100-pS) unitary conductance (Crawford et al., 1991; Géléoc et al., 1997; Ricci et al., 2003; Beurg et al., 2006), are located at the tops of the stereocilia (Beurg et al., 2009). These channels are activated by tension in the tip links (Pickles et al., 1984; Furness and Hackney, 1985), fine extracellular strands that connect the top of each stereocilium with the side wall of its taller neighbor. Although analyses of mutations associated with deafness in humans and mice have enabled the elucidation of some of the molecular apparatus underlying transduction, including the composition and anchoring of the tip links (Richardson et al., 2011; Kazmierczak and Müller, 2012), the identity of the MT channel remains controversial. However, recent work has indicated that two isoforms of the transmembrane channel–like family, Tmc1 and Tmc2, play a central role in hair cell mechanotransduction (Kawashima et al., 2011). The "*dn*" and "*Beethoven*" mutations in the *Tmc1* gene are associated with hearing loss (Steel and Bock, 1980; Kurima et al., 2002; Vreugde et al., 2002), but it has been unclear whether deafness stems from lack of MT channel function or is secondary to a developmental defect (Marcotti et al., 2006). Double knockouts of Tmc1 and Tmc2 abolish MT currents in both auditory and vestibular epithelia, a phenotype that can be rescued by transfection with either Tmc1 or Tmc2 mRNA (Kawashima et al., 2011). Although these results argue for a central role for Tmc1 and Tmc2 in hair cell mechanotransduction, it remains uncertain whether the MT current vanishes in *Tmc1−/−* (Marcotti et al., 2006; Kawashima et al., 2011).

The mammalian cochlea separates acoustic frequencies along its length so that auditory nerve fibers emanating from different regions are tuned to disparate frequencies, responding preferentially to high pitched tones at the base and low pitched ones at the apex (Fettiplace and Hackney, 2006). This systematic change in best frequency along the length of the cochlea, referred to as the tonotopic organization, stems from gradients in numerous properties including the dimensions

Correspondence to Robert Fettiplace: fettiplace@wisc.edu

Abbreviations used in this paper: IHC, inner hair cell; MT, mechanotransducer; OHC, outer hair cell.

The Rockefeller University Press $30.00
J. Gen. Physiol. Vol. 141 No. 1 141–148
www.jgp.org/cgi/doi/10.1085/jgp.201210913

of the cochlear partition and the ion channel complement of the outer hair cells (OHCs). Among these variables is the single-channel conductance of the MT channel, which, in mammals, increases from apex to base in OHCs but remains constant in inner hair cells (IHCs) (Beurg et al., 2006). This suggests that multiple isoforms of the MT channel protein may be differentially distributed along the mammalian cochlea. Here, we characterized MT channel properties in both wild-type mice and Tmc mutants and found that, in the first postnatal week, there is also a tonotopic gradient in the Ca^{2+} selectivity of the OHC MT channel that can be modified by mutations in Tmc1 or Tmc2. Our results suggest that the Tmc proteins specify the subunit composition of the MT channel.

MATERIALS AND METHODS

Animal preparation

MT currents were recorded in OHCs and IHCs in isolated organs of Corti of mice between 0 and 10 d postnatal (P0–P10, where P0 is the birth date) using methods described previously (Beurg et al., 2006). For initial characterizations in wild-type animals, both outbred CD-1 and inbred CBA/J mice were used, with the majority of measurements obtained on P4–P7 mice at the apex and P2–P5 mice at the base, ages at which the MT current was maximal at each position (Fig. 1, C and D). Mutation in Tmc1 was achieved with *dn* mice (CBA.Cg-*Tmc1*^{dn}/AjgJ; The Jackson Laboratory), which contain a deletion of exon 14 and are on a CBA/J background. The Tmc2 mutants (B6;129S5-*Tmc2*^{tm1Lex}/Mmucd), in which exon 1 is deleted, were obtained from the Mutant Mouse Regional Resource Center (University of California, Davis, Davis, CA). These were supplied as heterozygotes and bred with CBA/J mice through three generations to put them on the same background as the Tmc1 mutants, although the limited number of generations may be insufficient to ensure that both Tmc1 and Tmc2 had identical backgrounds. Both male and female mice of all strains were used. Mice were genotyped from tail clips using procedures and primer sets recommended by the suppliers.

Mice were killed by decapitation using methods approved by the Institutional Animal Care and Use Committee of the University of Wisconsin-Madison according to current National Institutes of Health guidelines. Excised apical, middle, or basal cochlear turns were fixed under ties of dental floss in a recording chamber mounted on a microscope (Axioskop FS; Carl Zeiss) and viewed through a 40× water-immersion objective (Carl Zeiss). The chamber was perfused with artificial perilymph of the following composition (mM): 150 NaCl, 6 KCl, 1.5 $CaCl_2$, 2 Na-pyruvate, 8 D-glucose, and 10 Na-HEPES, pH 7.4. The effect of endolymphatic Ca^{2+} was examined by changing the solution around the hair bundle using a nearby puffer pipette to one containing (mM): 150 KCl, 0.02 $CaCl_2$ (buffered with 4 HEDTA), 2 Na-pyruvate, 8 D-glucose, and 10 HEPES, pH 7.4. The puffer pipette was positioned ~30 µm from the target and directed along the cochlear axis so that the flow did not directly stimulate the bundle.

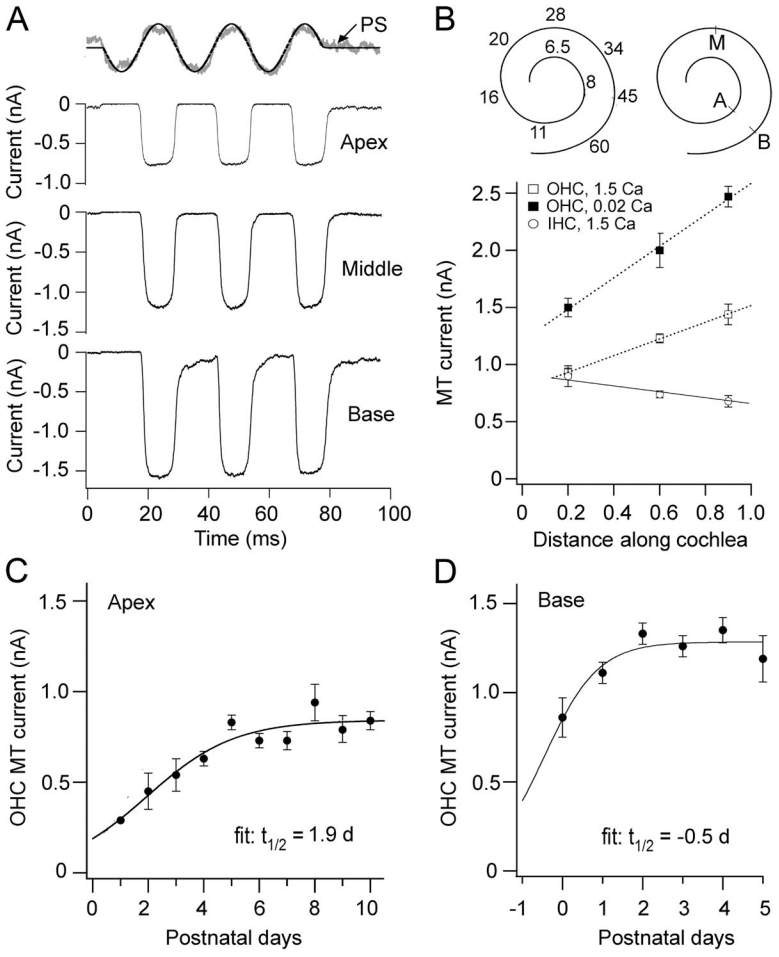

Figure 1. Tonotopic variation in MT current amplitudes. (A) Examples of MT currents in apical, middle, and basal OHCs in response a 40-Hz fluid jet stimulus. The time course of hair bundle motion for the apical cell is shown by the noisy photodiode signal (PS) superimposed on the driving voltage to the fluid jet piezoelectric disc. (B; top) Mouse cochlea schematics showing the tonotopic map with characteristic frequencies in kilohertz (left) and the approximate location of the apical (A), middle (M), and basal (B) recordings (right); map is taken from data of Müller et al. (2005). (Bottom) Mean MT current (± SEM) as a function of cochlear location for OHCs (open squares) and IHCs (open circles) in perilymph containing Na^+, 1.5 mM Ca^{2+}, and for OHCs (closed squares) in endolymph containing K^+, 0.02 mM Ca^{2+}. Abscissa is the distance from the apex divided by the total length of the cochlea. Each point is the average of five or more measurements in neonatal mice (P2–P6; holding potential of −84 mV). (C and D) Development of OHC MT current at apex and base; mean current I ± SEM plotted as a function of number of days postnatal. Results are fitted with a sigmoid equation, $I = I_{max}/(1 + \exp(-(t - t_{0.5})/t_s))$, to give a time to half-maximum ($t_{0.5}$) and maximum current (I_{max}) of 1.9 d and 0.84 nA (apex) and −0.5 d and 1.28 nA (base); the slope, t_s, is 1.4 (apex) and 0.7 (base). Number of cells averaged in C: P1, $n = 2$; P2, $n = 4$; P3, $n = 9$; P4, $n = 21$; P5, $n = 16$; P6, $n = 26$; P7, $n = 11$; P8, $n = 7$; P9, $n = 9$; P10, $n = 10$. Number of cells averaged in D: P0, $n = 5$; P1, $n = 9$; P2, $n = 25$; P3, $n = 16$; P4, $n = 9$; P5, $n = 3$.

Whole-cell recording

Recordings were made from first or second row OHCs or from IHCs using borosilicate patch electrodes connected to an amplifier (Axopatch 200A; Axon Instruments), and currents were low-pass filtered at the amplifier output at 10 kHz. Patch electrodes were filled with a solution containing (mM): 135 CsCl, 3 MgATP, 10 Tris phosphocreatine, 1 EGTA, and 10 Cs-HEPES, pH 7.2; in some experiments, 3 mM BAPTA rather than EGTA was used as the intracellular Ca^{2+} buffer. Membrane potentials were corrected for a liquid junction potential and for the voltage drop across the uncompensated series resistance. Most voltage-clamp protocols are referred to a holding potential of −84 mV. Values are given as mean ± 1 SEM, and $P < 0.05$ indicates statistically significant difference on a two-tailed Student's *t* test. All experiments were performed at room temperature of 21–25°C.

Reversal potentials

Reversal potentials (V_{REV}) were determined by using an extracellular solution containing (mM): 100 $CaCl_2$, 20 *N*-methylglucamine, 6 Tris, and 10 glucose, adjusted with HCl to pH 7.4, in both the fluid jet and the puffer pipette. Reversal potentials were corrected for a liquid junction potential of 9 mV. The relative Ca^{2+} permeability, P_{Ca}/P_{Cs}, was calculated from the Goldman–Hodgkin–Katz equation:

$$P_{Ca} / P_{Cs} = \{a_1[Cs^+] / 4a_2[Ca^{2+}]\}\bullet\{\exp(V_{REV}F/RT)\}\bullet\{1 + \exp(V_{REV}F/RT)\},$$

where RT/F has its usual meaning with a value at room temperature of 25.7 mV, $[Cs^+]$ and $[Ca^{2+}]$ are the concentrations of Cs^+ intracellularly (140 mM) and Ca^{2+} extracellularly (100 mM), and a_1 and a_2 are the published activity coefficients for Cs^+ (Partanen, 2010) and Ca^{2+} (Rard and Clegg, 1997), respectively. The analysis assumes that these are the only ions to which the MT channel is permeable and that the contributions of *N*-methylglucamine and Tris are negligible. Hair bundles were mechanically stimulated with a fluid jet from a pipette, with a tip diameter of 10–15 µm, driven by a 25-mm diameter piezoelectric disc (Johnson et al., 2011). The distance of the pipette tip from the bundle was adjusted to elicit a maximal MT current. When testing the effects of different Ca^{2+} concentrations, the fluid jet pipette was filled with a solution containing the relevant Ca^{2+}, and the perfusate around the hair bundle was also exchanged for the same Ca^{2+} solution in the puffer. During fluid jet stimulation, bundle motion was monitored by projecting an image of the bundle onto a pair of photodiodes (LD 2–5; Centronics) at a total magnification of 340 (Johnson et al., 2011).

RESULTS

MT currents in wild-type mice

We initially characterized the properties of the wild-type MT channel, seeking features that might reveal tonotopic differences in the ion conduction pathway or "pore" of the channel. MT currents were recorded from hair cells in isolated turns of neonatal (P2–P10) mouse cochleas in response to deflections of their stereociliary bundle, implemented with a fluid jet (Kros et al., 1992; Johnson et al., 2011) to minimize damage to the short bundles (Fig. 1 A). Measurements were obtained from organ of Corti segments at fractional distances (the longitudinal distance from the apex divided by the total length of the cochlea) of 0.2, 0.6, and 0.9 (Fig. 1 B), which will be referred to as apex, middle, and base, respectively. MT currents in OHCs increased in peak amplitude from apex to base, whereas IHC MT currents varied little across the three locations (Fig. 1 B), similar to results found in other rodents (Beurg et al., 2006; Jia et al., 2007). For the IHC currents there was a small decrease from apex to base, which might be partly accounted for by greater metabolic vulnerability of the basal hair cells and damage to or block of the MT channels, for example by Ca^{2+} loading. If this also occurred

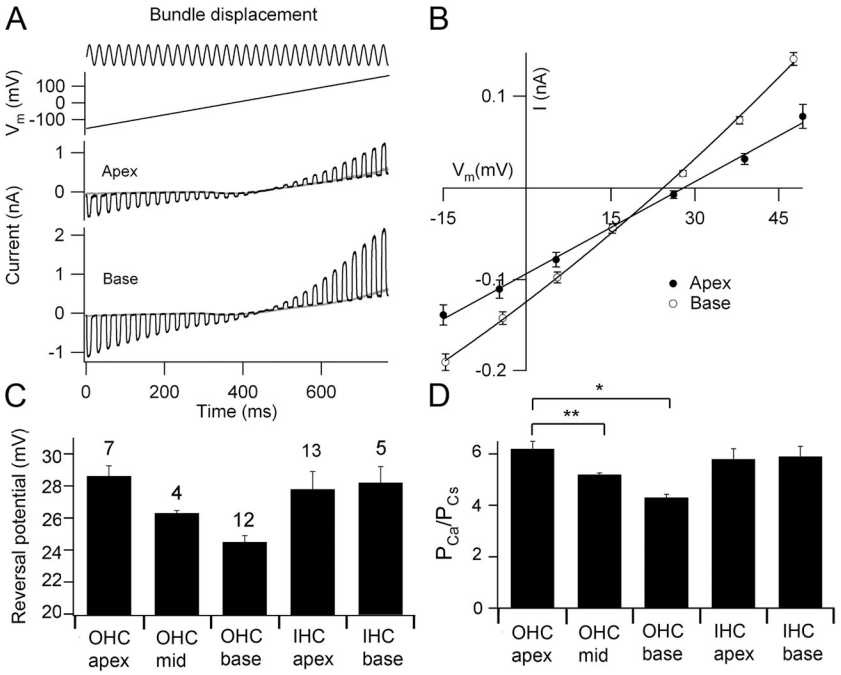

Figure 2. Reversal potentials and Ca^{2+} permeabilities in OHCs. (A) Combined hair bundle stimulus with a fluid jet and a voltage-ramp protocol. MT currents for OHCs at apex and at base are shown for hair bundle perfusate containing 100 mM Ca^{2+} and are superimposed on the response to the ramp alone. (B) Average current–voltage relationships for OHC MT currents for apical (closed circles) and for basal (open circles); each point is the mean ± 1 SEM. (C) Mean Ca^{2+} reversal potentials for OHC MT currents at apex, middle, and base, and IHCs at apex and base; the number of experiments is indicated above bars. (D) P_{Ca}/P_{Cs} calculated from reversal potentials in C for OHC MT currents at apex, middle, and base, and IHCs at apex and base. The value for the OHC base includes those using EGTA and BAPTA in the internal solution. OHC Ca^{2+} permeabilities differ significantly from each other: *, apex against base ($P = 0.00001$; *t* test); **, apex against middle ($P = 0.02$; *t* test). Mouse ages: P5 apical, P3 middle, and P2–P5 basal OHCs; P4–P7 apical and P2–P3 basal IHCs.

in OHCs, then the apex to base gradient in their current will be even larger. The tonotopic variation in the MT current was conserved if the OHC hair bundles were perfused with endolymph (K^+; 0.02 mM Ca^{2+}) to which they are normally exposed in vivo rather than the perilymph (Na^+; 1.5 mM Ca^{2+}), but at all locations the current amplitude was larger (Fig. 1 B), with the increase averaged over the three locations being 1.66 ± 0.06 (mean ± SEM). Tonotopic variation in the size of the macroscopic MT current and conductance in OHCs may be attributable to a combined increase in the single-channel conductance and the number of stereocilia (and hence channels) per bundle from apex to base (Beurg et al., 2006).

Ca^{2+} permeability of the MT channel

Variation in the pore region of the MT channel may be manifested as a difference in its ionic selectivity, especially that for Ca^{2+}, which is the most permeant ion. The Ca^{2+} permeability of the channel was determined from measurements of reversal potentials under conditions where Ca^{2+} was the sole permeant ion extracellularly and Cs^+ was the intracellular cation. The experimental protocol constituted a saturating hair bundle stimulus superimposed on a voltage ramp (Fig. 2 A). Changes in the amplitude of the MT current in the voltage region around the reversal potential were approximately linear with membrane potential (Fig. 2 B), enabling accurate interpolation of the reversal potential. The Ca^{2+} permeability, P_{Ca}/P_{Cs}, was calculated from the reversal potential, V_{REV}, using the Goldman–Hodgkin–Katz equation (see Materials and methods). For the OHCs, the reversal potential and relative Ca^{2+} permeability showed small but significant decreases from apex to base, whereas the values were invariant with position for the IHCs (Fig. 2, C and D). Thus, for OHCs, the mean P_{Ca}/P_{Cs} (± SEM) = 6.1 ± 0.7 (n = 7) at the apex, 5.2 ± 0.1 (n = 4) at the middle, and 4.6 ± 0.5 (n = 12) at the base. The three means were significantly different from each other (t test; $P < 0.02$). A concern is that the smaller permeability at the base may be caused by Ca^{2+} loading, but the inferred permeability for basal OHCs was unaffected when 3 mM BAPTA was used instead of 1 mM EGTA as the Ca^{2+} buffer in the intracellular solution (P_{Ca}/P_{Cs} = 4.2 ± 0.6; n = 9). The results were also unaffected by reversing the polarity of the voltage ramp, starting at a depolarized potential where the initial Ca^{2+} flux would be outward. The results demonstrate a tonotopic gradient in OHC channel properties from apex to base, but IHCs lack such a gradient either in Ca^{2+} permeability or MT current size.

Changes with development

The measurements reported so far were made on animals in the first neonatal week. The MT current grows in amplitude over the first few neonatal days, with development at the apex lagging the base by about 2–3 d (Waguespack et al., 2007; Lelli et al., 2009). In our measurements on

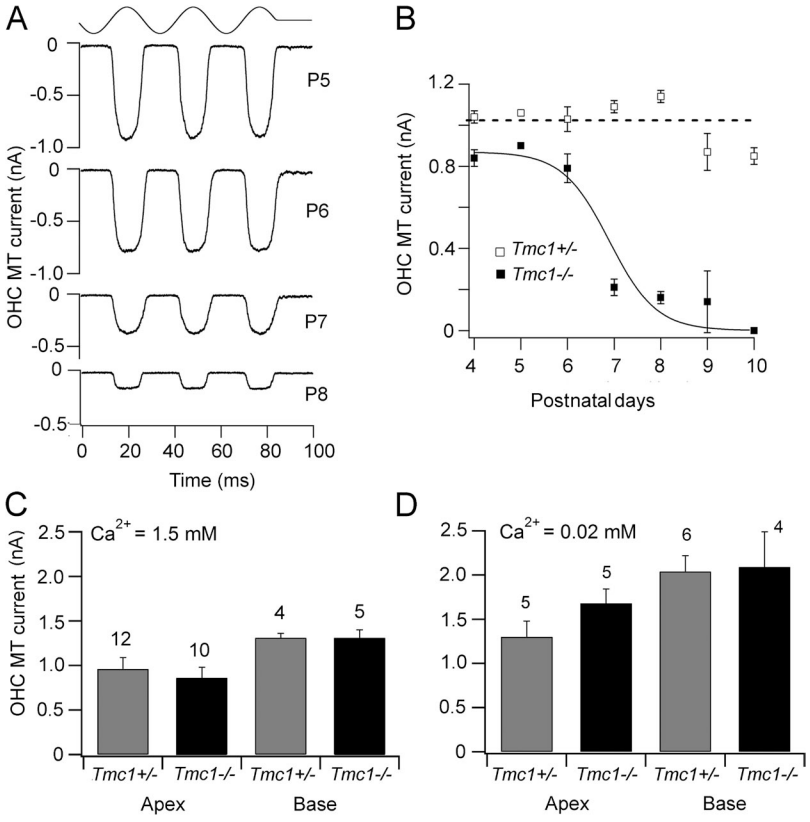

Figure 3. Developmental changes in OHC MT current in *Tmc1−/−*. (A) MT currents in apical OHCs at different postnatal ages (P5–P8) in *Tmc1−/−*. Representative currents recorded at each age are depicted. (B) Apical OHC MT current amplitudes at different postnatal ages (P4–P10) in *Tmc1−/−* (closed squares) and *Tmc1+/−* (open squares). Each point is the mean ± 1 SEM. Number of cells averaged: *Tmc1+/−*: P4, n = 9; P5, n = 1; P6, n = 2; P7, n = 4; P8, n = 4; P9, n = 6; P10, n = 10. Number of cells averaged: *Tmc1−/−*: P4, n = 5; P5, n = 1; P6, n = 4; P7, n = 4; P8, n = 4; P9, n = 5; P10, n = 10. (C) Collected MT amplitudes in 1.5 mM Ca^{2+} as a function of cochlear location in *Tmc1+/−* and *Tmc1−/−*. (D) Collected MT amplitudes in 0.02 mM Ca^{2+} as a function of cochlear location in *Tmc1+/−* and *Tmc1−/−*; holding potential of −84 mV. In both C and D, the ages of mice were P4–P6 for the apex and P2–P4 at the base; the number of experiments is indicated above bars.

wild-type mice, the OHC current became maximal by P2 at the base and P4 at the apex (Fig. 1, C and D). MT currents at the two locations were recorded at a postnatal age when the current had become maximal, but at this stage, cochlear hair cells are still relatively immature. For example, OHCs lack the somatic motor prestin (Belyantseva et al., 2000; Abe et al., 2007) as well as the KCNQ4 voltage-dependent K^+ conductance (Marcotti and Kros, 1999). These membrane proteins appear during the second postnatal week before the onset of hearing at about P12. During the second and third weeks, there are no further changes in the MT current amplitude (Fig. 1, C and D; Kennedy et al., 2003), but we did find changes in the OHC MT channel Ca^{2+} permeability: the apical permeability decreased with development from (mean ± SEM) 6.1 ± 0.7 (n = 7; P5–P6) to 4.6 ± 0.1 (n = 6; P8–P10), now making it similar to that at the base, which was 4.2 ± 0.2 (n = 4; P8). In the older animals, the Ca^{2+} permeabilities in apical and basal OHCs were no longer significantly different (t test; P = 0.38), implying that the gradient in OHC MT channel Ca^{2+} permeability is a developmental feature. In contrast to the OHCs, no such developmental change was seen in IHCs. The Ca^{2+} permeability in apical IHCs was 5.7 ± 0.4 (n = 13; P4–P7) and 5.8 ± 0.4 (n = 5; P8–P9). Thus, in the P8–P10 mice, after the developmental switch, the Ca^{2+} permeability of the MT channel in IHCs is larger than that in OHCs. This permeability difference between these two cell types agrees with previous results found in rat cochleas at a similar developmental age (Beurg et al., 2006).

Tmc1 and Tmc2 knockouts

We next investigated the effects on the tonotopic organization of *Tmc1*−/− and *Tmc2*−/− mice, the former (*dn*) being a recessive mutation that lacks exon 14 in the *Tmc1* gene, and the latter being a recessive mutation with a deletion of exon 1 of the *Tmc2* gene. In *Tmc1*−/−, there was little or no effect on the OHC MT current amplitude up until about P6 (Fig. 3 A), but beyond this time point, the current declined to zero by P10, but it was maintained in the heterozygotes (Fig. 3 B). For IHCs, significant though reduced MT currents could still be recorded in *Tmc1*−/− at P9: the mean current was 0.35 ± 0.02 nA (n = 3) in the knockout compared with 0.66 ± 0.07 nA (n = 3) in the heterozygotes. Although

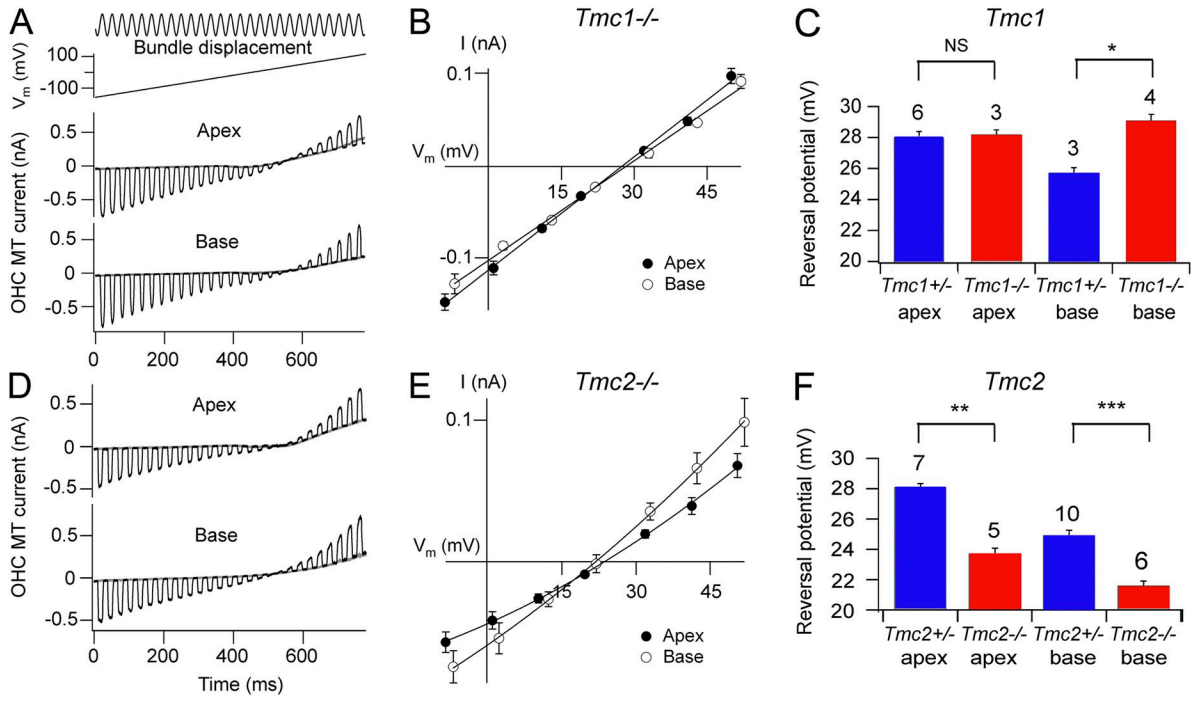

Figure 4. Ca^{2+} reversal potentials for OHC MT currents in *Tmc1*−/− and *Tmc2*−/−. (A) MT currents in Tmc1 knockout for OHCs at apex and at base are shown as in Fig. 3 for hair bundle perfusate containing 100 mM Ca^{2+}. (B) Tmc1 knockouts: average current–voltage relationships for OHC MT currents around the reversal potential for apical (closed circles; n = 3) and basal (open circles; n = 4). (C) Collected MT reversal potentials for *Tmc1*+/− and *Tmc1*−/− at apex and base; the number of experiments is indicated above bars. With t test, NS, not significantly different, P = 0.82; *, significantly different, P = 0.0016. The mean *Tmc1*−/− at apex and base is not significantly different (P = 0.18). (D) MT currents in Tmc2 knockout for OHCs at apex and base as in A for hair bundle perfusate containing 100 mM Ca^{2+}. (E) Tmc2 knockouts: average current–voltage relationships for OHC MT currents around the reversal potential for apical (closed circles; n = 5) and basal (open circles; n = 6). Note that in B and E, the apical and basal plots have similar reversal potentials. (F) Collected MT reversal potentials for *Tmc2*+/− and *Tmc2*−/− at apex and base. With t test, **, significantly different, P = 10^{-6}; ***, significantly different, P = 0.0003. All measurements were made on P2–P5 animals.

loss of transduction in OHCs may account for the deafness phenotype in *dn* mice, it disagrees with the observation of Marcotti et al. (2006), who were still able to record large OHC MT currents in *dn* mice at P8. The reason for this discrepancy is unclear, but it might result from differences in the genetic background: the mice used by Marcotti et al. (2006) were from the original *dn* stock and were maintained on an unknown background. However, in accord with our results, Kawashima et al. (2011) found an ~40% reduction in the apical OHC current amplitude in P5–P7 *Tmc1*−/− mice.

The properties of the MT current before P6 in the *Tmc1*−/− mice were similar to those documented for the wild type or heterozygotes (Fig. 3, C and D). The current amplitudes at −84 mV were similar to wild type in perilymph (mean ± SEM = 0.86 ± 0.12 nA, n = 10, apex; 1.31 ± 0.09 nA, n = 5, base; Ca^{2+} = 1.5 mM), and also the current increased up to twofold upon exposing the bundle to endolymph (mean ± SEM = 1.68 ± 0.16 nA, n = 5, apex; 2.09 ± 0.4 nA, n = 4, base; Ca^{2+} = 0.02 mM). The tonotopic gradient in current amplitude was not significantly different between heterozygotes and *Tmc1*−/− mice over the time period before decline in the current in the knockout.

To explore further any differences in the Tmc1 knockouts, we measured the Ca^{2+} permeability of the MT channel and found that the gradient in OHC channel permeability was eliminated in the *Tmc1*−/− mice but not in the heterozygotes (Fig. 4, A–C). Abolition of the gradient occurred because the permeability at the base increased to become comparable to that at apex. Mean values (± SEM) for the Ca^{2+} permeability in the *Tmc1*−/− mice were 5.9 ± 0.2 (n = 3) at the apex and 6.3 ± 0.2 (n = 4) at the base. The Ca^{2+} permeability of the channel was also determined in *Tmc2*−/− mice. Robust MT currents could still be recorded in the neonatal *Tmc2*−/− mice. In perilymph at −84 mV, the apical OHC current was as follows: 0.35 ± 0.03 nA (n = 4) in *Tmc2*−/− compared with 1.02 ± 0.06 nA (n = 9) in *Tmc2*+/− at P4; 0.97 ± 0.05 nA (n = 4) in *Tmc2*−/− compared with 0.8 ± 0.07 nA (n = 3) in *Tmc2*+/− at P5; and 0.74 ± 0.10 nA (n = 3) in *Tmc2*−/− compared with 0.95 ± 0.05 nA (n = 2) in *Tmc2*+/− at P8. However, in *Tmc2*−/− mice, the MT channel Ca^{2+} permeability decreased at the apex and also to some extent at the base compared with the wild type or the heterozygotes (Fig. 4, D–F). Mean values (± SEM) for the Ca^{2+} permeability in the *Tmc2*−/− mice were 4.4 ± 0.1 (n = 5) at the apex and 3.7 ± 0.1 (n = 6) at the base. Thus, loss of Tmc2 reduces the Ca^{2+} permeability of the channel in both apical and basal OHCs. Knockout of Tmc2 had a similar effect on the apical IHCs both before (P4–P7) and after (P8–P9) the first postnatal week (Fig. 5). For example, the MT channel Ca^{2+} permeability in wild type was 5.7 ± 0.4 (n = 13) and in *Tmc2*−/− was 4.5 ± 0.2 (n = 6), which are significantly different (t test; P < 0.02) for P4–P7. A similar reduction in permeability with the knockout was seen in P8–P9 animals, indicating that Tmc2 is still present in the IHCs at that time. No such change was seen with the *Tmc1*−/− for which the IHCs retained their higher permeability (mean = 6.6 ± 0.6; n = 3).

DISCUSSION

We have characterized the currents flowing through the MT channels and their relative Ca^{2+} permeability in

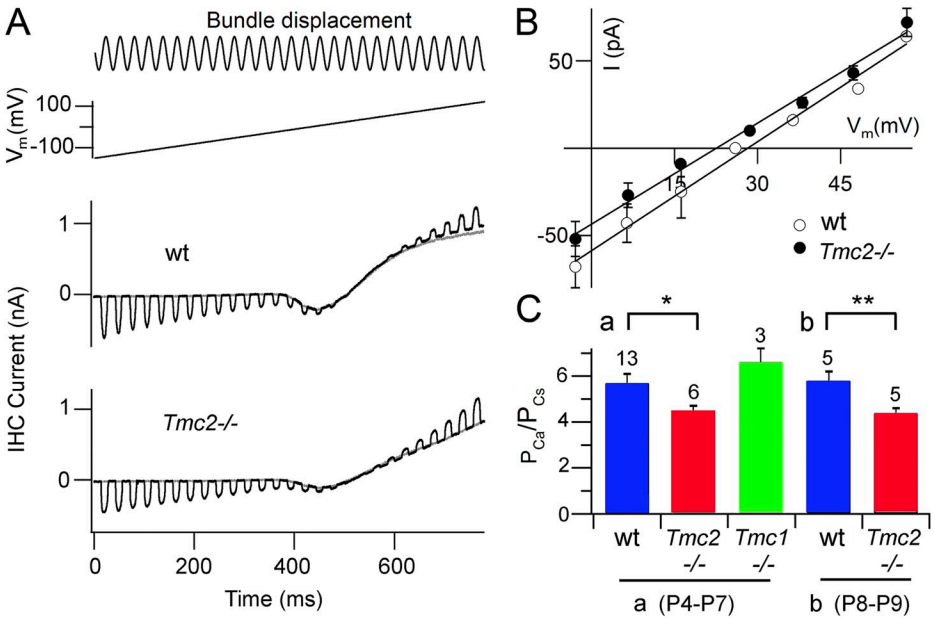

Figure 5. Ca^{2+} reversal potentials for IHC MT currents in *Tmc1*−/− and *Tmc2*−/−. (A) MT currents in wild type and Tmc2 knockout for apical IHCs from P8 mice are shown as in Fig. 4 for hair bundle perfusate containing 100 mM Ca^{2+}. Note the inward Ca^{2+} current. (B) Average current–voltage relationships for IHC MT currents around the reversal potential for wild type (wt, open circles; n = 2) and *Tmc2*−/− (closed circles; n = 3), both in P8 mice. (C) Collected MT reversal potentials for *Tmc1*−/− and *Tmc2*−/−, for (a) P4–P7 and (b) P8–P9 mice; the number of experiments is indicated above bars. With t test, wild type and *Tmc2*−/− are significantly different in the younger (*, P = 0.012) and older (**, P = 0.005) animals. The mean wild type in (a) and (b) are not significantly different (t test; P = 0.64), and the wild type in (a) is not significantly different from the *Tmc1*−/− (t test; P = 0.16).

OHCs and IHCs along the mouse cochlea. Differences in Ca^{2+} permeability are likely to be the most robust indicator of a tonotopic variation in the ion conduction pathway or "pore" of the channel. Although small, the differences we observed under various conditions were reproducible and permit several conclusions. First, the Ca^{2+} permeability measurements show a gradation from apex to base in OHC MT channels, whereas this gradient is absent in IHCs, with similar permeabilities at the apex and base. Second, the gradient exists only during the first neonatal week, and thereafter (up to at least P10) the Ca^{2+} permeability decreases in apical OHCs to become the same as basal OHCs, whereas the IHCs are unchanged. Third, the Ca^{2+} permeability is susceptible to mutations in Tmc1 and Tmc2. Variations in the channel's Ca^{2+} permeability were not accompanied by any striking changes in the MT current amplitude under any of the conditions studied. For example, once the MT currents became maximal at about P2 and P4 at the base and apex, respectively, they remained constant despite changes in Ca^{2+} permeability after the first neonatal week. The MT current amplitudes were similar to those reported in other rodents, with a tonotopic gradient for OHCs but no such gradient in IHCs (He et al., 2004; Beurg et al., 2006; Jia et al., 2007; Stauffer and Holt, 2007).

A clue to the variability arises from the results with the Tmc1 and Tmc2 mutants. Knockout of Tmc1 increased the Ca^{2+} permeability in basal OHCs, whereas knockout of Tmc2 reduced the permeability in apical (and to some extent also basal) OHCs and in IHCs. It is conceivable that the Tmc proteins are chaperones or trafficking proteins that specify channel composition. Indeed, Tmc6 and Tmc8 (also referred to as EVER1 and EVER2) are cytoplasmic proteins that interact with a zinc transporter to regulate Zn^{2+} levels in keratinocyte nucleoli (Lazarczyk et al., 2008). However, the results would also be consistent with the notion that Tmc1 and Tmc2 are in fact channel subunits able to contribute to the pore region, with Tmc1 being more important at the base and Tmc2 endowing the higher Ca^{2+} permeability at the apex and in IHCs. In line with this conclusion, the reduction in permeability of apical OHCs later than P6 may be accounted for by loss of Tmc2, which is downregulated in the cochlea at this time (Kawashima et al., 2011). It is also consistent with the loss of the OHC MT current in *Tmc1−/−*, which occurs at about the same time. Indeed, the time course of disappearance of the current (Fig. 3 B) perhaps more precisely reflects loss of Tmc2 protein, which may be slightly delayed with respect to the decline in the message after P5 (see Fig. 1 B of Kawashima et al., 2011), with the delay reflecting the time course of MT channel turnover.

The results raise an important question concerning the functional significance of a change in MT channel composition and Ca^{2+} permeation during development. One possible explanation is that up until P6, cochlear hair cells are nonspecialized and the properties measured reflect those of the generic hair cell. In this context, it is pertinent that Tmc2 is retained in the vestibular end organs in the adult (Kawashima et al., 2011), and Tmc2 knockout, with or without Tmc1, substantially reduces MT currents in utricular type II hair cells, which might be regarded as less specialized than cochlear OHCs. The time point around P7 coincides with refining the OHC phenotype, including acquisition of prestin and the onset of electromotility (Belyantseva et al., 2000; Abe et al., 2007), the appearance of new voltage-dependent K^+ currents ($I_{K,n}$; Marcotti and Kros, 1999), and changes in the pattern of innervation. Interestingly, failure to develop the adult hair cell voltage-dependent K^+ channels was a conspicuous feature of the *Tmc1 dn* mutant (Marcotti et al., 2006). The causal relationship between a functional MT channel and subsequent maturation will be a worthwhile problem to address.

This work is supported by grant RO1 DC01362 from the National Institute on Deafness and other Communication Disorders to R. Fettiplace.

Edward N. Pugh Jr. served as editor.

Submitted: 16 October 2012
Accepted: 10 December 2012

REFERENCES

Abe, T., S. Kakehata, R. Kitani, S. Maruya, D. Navaratnam, J. Santos-Sacchi, and H. Shinkawa. 2007. Developmental expression of the outer hair cell motor prestin in the mouse. *J. Membr. Biol.* 215:49–56. http://dx.doi.org/10.1007/s00232-007-9004-5

Belyantseva, I.A., H.J. Adler, R. Curi, G.I. Frolenkov, and B. Kachar. 2000. Expression and localization of prestin and the sugar transporter GLUT-5 during development of electromotility in cochlear outer hair cells. *J. Neurosci.* 20:RC116.

Beurg, M., M.G. Evans, C.M. Hackney, and R. Fettiplace. 2006. A large-conductance calcium-selective mechanotransducer channel in mammalian cochlear hair cells. *J. Neurosci.* 26:10992–11000. http://dx.doi.org/10.1523/JNEUROSCI.2188-06.2006

Beurg, M., R. Fettiplace, J.H. Nam, and A.J. Ricci. 2009. Localization of inner hair cell mechanotransducer channels using high-speed calcium imaging. *Nat. Neurosci.* 12:553–558. http://dx.doi.org/10.1038/nn.2295

Corey, D.P., and A.J. Hudspeth. 1979. Ionic basis of the receptor potential in a vertebrate hair cell. *Nature.* 281:675–677. http://dx.doi.org/10.1038/281675a0

Crawford, A.C., M.G. Evans, and R. Fettiplace. 1991. The actions of calcium on the mechano-electrical transducer current of turtle hair cells. *J. Physiol.* 434:369–398.

Fettiplace, R., and C.M. Hackney. 2006. The sensory and motor roles of auditory hair cells. *Nat. Rev. Neurosci.* 7:19–29. http://dx.doi.org/10.1038/nrn1828

Furness, D.N., and C.M. Hackney. 1985. Cross-links between stereocilia in the guinea pig cochlea. *Hear. Res.* 18:177–188. http://dx.doi.org/10.1016/0378-5955(85)90010-3

Géléoc, G.S., G.W. Lennan, G.P. Richardson, and C.J. Kros. 1997. A quantitative comparison of mechanoelectrical transduction in vestibular and auditory hair cells of neonatal mice. *Proc. Biol. Sci.* 264:611–621. http://dx.doi.org/10.1098/rspb.1997.0087

He, D.Z.Z., S. Jia, and P. Dallos. 2004. Mechanoelectrical transduction of adult outer hair cells studied in a gerbil hemicochlea. *Nature.* 429:766–770. http://dx.doi.org/10.1038/nature02591

Jia, S., P. Dallos, and D.Z. He. 2007. Mechanoelectric transduction of adult inner hair cells. *J. Neurosci.* 27:1006–1014. http://dx.doi.org/10.1523/JNEUROSCI.5452-06.2007

Johnson, S.L., M. Beurg, W. Marcotti, and R. Fettiplace. 2011. Prestin-driven cochlear amplification is not limited by the outer hair cell membrane time constant. *Neuron.* 70:1143–1154. http://dx.doi.org/10.1016/j.neuron.2011.04.024

Kawashima, Y., G.S. Géléoc, K. Kurima, V. Labay, A. Lelli, Y. Asai, T. Makishima, D.K. Wu, C.C. Della Santina, J.R. Holt, and A.J. Griffith. 2011. Mechanotransduction in mouse inner ear hair cells requires transmembrane channel-like genes. *J. Clin. Invest.* 121:4796–4809. http://dx.doi.org/10.1172/JCI60405

Kazmierczak, P., and U. Müller. 2012. Sensing sound: molecules that orchestrate mechanotransduction by hair cells. *Trends Neurosci.* 35:220–229. http://dx.doi.org/10.1016/j.tins.2011.10.007

Kennedy, H.J., M.G. Evans, A.C. Crawford, and R. Fettiplace. 2003. Fast adaptation of mechanoelectrical transducer channels in mammalian cochlear hair cells. *Nat. Neurosci.* 6:832–836. http://dx.doi.org/10.1038/nn1089

Kros, C.J., A. Rüsch, and G.P. Richardson. 1992. Mechano-electrical transducer currents in hair cells of the cultured neonatal mouse cochlea. *Proc. Biol. Sci.* 249:185–193. http://dx.doi.org/10.1098/rspb.1992.0102

Kurima, K., L.M. Peters, Y. Yang, S. Riazuddin, Z.M. Ahmed, S. Naz, D. Arnaud, S. Drury, J. Mo, T. Makishima, et al. 2002. Dominant and recessive deafness caused by mutations of a novel gene, TMC1, required for cochlear hair-cell function. *Nat. Genet.* 30:277–284. http://dx.doi.org/10.1038/ng842

Lazarczyk, M., C. Pons, J.A. Mendoza, P. Cassonnet, Y. Jacob, and M. Favre. 2008. Regulation of cellular zinc balance as a potential mechanism of EVER-mediated protection against pathogenesis by cutaneous oncogenic human papillomaviruses. *J. Exp. Med.* 205:35–42. http://dx.doi.org/10.1084/jem.20071311

Lelli, A., Y. Asai, A. Forge, J.R. Holt, and G.S. Géléoc. 2009. Tonotopic gradient in the developmental acquisition of sensory transduction in outer hair cells of the mouse cochlea. *J. Neurophysiol.* 101:2961–2973. http://dx.doi.org/10.1152/jn.00136.2009

Marcotti, W., and C.J. Kros. 1999. Developmental expression of the potassium current IK,n contributes to maturation of mouse outer hair cells. *J. Physiol.* 520:653–660. http://dx.doi.org/10.1111/j.1469-7793.1999.00653.x

Marcotti, W., A. Erven, S.L. Johnson, K.P. Steel, and C.J. Kros. 2006. Tmc1 is necessary for normal functional maturation and survival of inner and outer hair cells in the mouse cochlea. *J. Physiol.* 574:677–698. http://dx.doi.org/10.1113/jphysiol.2005.095661

Müller, M., K. von Hünerbein, S. Hoidis, and J.W. Smolders. 2005. A physiological place-frequency map of the cochlea in the CBA/J mouse. *Hear. Res.* 202:63–73. http://dx.doi.org/10.1016/j.heares.2004.08.011

Ohmori, H. 1985. Mechano-electrical transduction currents in isolated vestibular hair cells of the chick. *J. Physiol.* 359:189–217.

Partanen, J.I. 2010. Re-evaluation of the thermodynamic activity quantities in aqueous rubidium and cesium chloride solutions at 25°C. *J. Chem. Eng. Data.* 55:249–257. http://dx.doi.org/10.1021/je900320r

Pickles, J.O., S.D. Comis, and M.P. Osborne. 1984. Cross-links between stereocilia in the guinea pig organ of Corti, and their possible relation to sensory transduction. *Hear. Res.* 15:103–112. http://dx.doi.org/10.1016/0378-5955(84)90041-8

Rard, J.A., and S.L. Clegg. 1997. Critical evaluation of the thermodynamic properties of aqueous calcium chloride. 1. Osmotic and activity coefficients of 0–10.77 mol · kg^{-1} aqueous calcium chloride solutions at 298.15 K and correlation with extended Pitzer ion-interaction models. *J. Chem. Eng. Data.* 42:819–849. http://dx.doi.org/10.1021/je9700582

Ricci, A.J., A.C. Crawford, and R. Fettiplace. 2003. Tonotopic variation in the conductance of the hair cell mechanotransducer channel. *Neuron.* 40:983–990. http://dx.doi.org/10.1016/S0896-6273(03)00721-9

Richardson, G.P., J.B. de Monvel, and C. Petit. 2011. How the genetics of deafness illuminates auditory physiology. *Annu. Rev. Physiol.* 73:311–334. http://dx.doi.org/10.1146/annurev-physiol-012110-142228

Stauffer, E.A., and J.R. Holt. 2007. Sensory transduction and adaptation in inner and outer hair cells of the mouse auditory system. *J. Neurophysiol.* 98:3360–3369. http://dx.doi.org/10.1152/jn.00914.2007

Steel, K.P., and G.R. Bock. 1980. The nature of inherited deafness in *deafness* mice. *Nature.* 288:159–161. http://dx.doi.org/10.1038/288159a0

Vreugde, S., A. Erven, C.J. Kros, W. Marcotti, H. Fuchs, K. Kurima, E.R. Wilcox, T.B. Friedman, A.J. Griffith, R. Balling, et al. 2002. Beethoven, a mouse model for dominant, progressive hearing loss DFNA36. *Nat. Genet.* 30:257–258. http://dx.doi.org/10.1038/ng848

Waguespack, J., F.T. Salles, B. Kachar, and A.J. Ricci. 2007. Stepwise morphological and functional maturation of mechanotransduction in rat outer hair cells. *J. Neurosci.* 27:13890–13902. http://dx.doi.org/10.1523/JNEUROSCI.2159-07.2007